Rathod, H.J., Asim, U.B., Radovic, M. and Srivastava, A., 2024. Micromechanics of kink-band formation in bimetallic layered composites. International Journal of Solids and Structures, 286,

p.112566.

Micromechanics of kink-band formation in bimetallic layered composites

Hemant J. Rathod, Umair Bin Asim, Miladin Radovic, Ankit Srivastava\*

Department of Materials Science and Engineering, Texas A&M University, College Station, TX

77845, USA

\*Corresponding author.

3003 TAMU, College Station, TX 77843, USA

Email address: ankit.sri@tamu.edu (A. Srivastava)

Abstract

Bimetallic layered composites with ultrathin layers possess high strength and hardness, excellent

shock resistance, and radiation damage tolerance. However, they are prone to deformation

localization and readily form kink-bands when subjected to layer parallel compression. Following

this, we carried out extensive plane strain finite element finite deformation analyses to understand

and rationalize the experimentally observed kink-band formation in these composites. In the

calculations, both constituent materials were assumed to follow a rate-independent isotropic

elastic-plastic constitutive relation with an ad-hoc thickness dependent yield strength. Our results

demonstrate that in these composites, layer refinement, together with the strength differential

between the layers of the constituent materials, is sufficient to trigger kink-banding. Importantly,

this phenomenon occurs even in the absence of elastically stiff layers, geometrical imperfections

(such as waviness of the layers), and extreme plastic anisotropy within the layers. Additionally,

we performed parametric studies to investigate the individual effects of layer thickness, strength differential between the two constituent materials, and strain-hardenability of the materials on kink-band formation. The outcomes of our parametric studies reveal that the strain-hardenability of the constituent materials stabilizes the formation of kink-bands. Furthermore, it leads to a transition from the abrupt formation of through-width kink-bands to the onset and propagation of stable inclined wedge-shaped kink-bands, similar to the experimental observations.

#### **Keywords**

Composite materials; Compression; Elastic plastic solids; Finite element; Instability

#### 1. Introduction

Bimetallic layered composites, such as Copper – Niobium, Copper – Chromium, Copper – Nickel (Misra et al., 1998) with layer thickness less than 100 nm have been shown to possess strength and hardness levels at least an order of magnitude greater than their constituents (Beyerlein et al., 2013b); and have also been shown to possess excellent shock resistance (Han et al., 2014) and radiation damage tolerance (Beyerlein et al., 2013a; Han et al., 2013). These composites are in general fabricated using severe plastic deformation techniques such as accumulative roll bonding (Del Valle et al., 2005; Saito et al., 1999) and equal channel angular extrusion (Valiev and Langdon, 2006; Xue et al., 2007). Nevertheless, their microstructure is found to be very stable even under extreme environments (Mara et al., 2008; Mara et al., 2010b; Misra et al., 2007; Misra et al., 2004). For example, the layer structure, thickness, interface characteristics and overall

texture of Copper (Cu) – Niobium (Nb) bimetallic layered composite with ~35 nm layer thickness were found to be stable up to 700°C for ~16 hours (Carpenter et al., 2013). This is due to the selection of well-bonded interfaces with low formation energy in these materials during fabrication (Beyerlein et al., 2013b; Carpenter et al., 2012; Mara and Beyerlein, 2014).

The bimetallic layered composites are, however, prone to deformation localization (Beyerlein et al., 2013b; Mara et al., 2010a; Tian and Zhang, 2013; Yan et al., 2013) even during the fabrication process (Ardeljan et al., 2014; Carpenter et al., 2015). Deformation localization in these composites has been shown to occur by two mechanisms (Nizolek et al., 2021). The first mechanism is shear-banding which leads to intense plastic deformation in narrow bands (Hong et al., 2010; Zheng et al., 2014). The second mechanism is the formation of kink-bands in bimetallic layered composites with ultrathin layers (Nizolek et al., 2017; Nizolek et al., 2015; Zhang et al., 2022). Deformation by these two mechanisms is observed under distinct loading conditions, shearbands form when the composite is compressed normal to the layers whereas kink-bands form when the composite is compressed parallel to the layers (Nizolek et al., 2021). Out of these two, shearband formation is considered to be detrimental as it leads to deformation localization without bound and monotonic decrease in the load carrying capacity of the material (Hong et al., 2010; Mara et al., 2010a; Zheng et al., 2014). On the contrary, kink-band formation has been found to be non-detrimental as it can lead to enhanced deformability and toughness of these composites (Ardeljan et al., 2018; Nizolek et al., 2015; Nizolek et al., 2021).

Kink-band formation is not limited to bimetallic layered composites and has been observed in a variety of materials that exhibit structural and/or material anisotropy, for example, fiber-reinforced

composites (Berg and Salama, 1973; Evans and Adler, 1978; Fleck and Budiansky, 1991; Jensen and Christoffersen, 1997; Moran et al., 1995; Vogler and Kyriakides, 2001), oriented polymers (Attenburrow and Bassett, 1979; Robertson, 1969), geological materials (Anderson, 1968; Kronenberg et al., 1990; Paterson and Weiss, 1966), freshwater ice (Manley and Schulson, 1997), wood (Poulsen et al., 1997), hexagonal closed packed (HCP) single crystals of Cadmium (Orowan, 1942) and Zinc (Cornwell et al., 1970; Crocker and Abell, 1976; Frank and Stroh, 1952; Hagihara et al., 2016; Hess and Barrett, 1949), and MAX phases (Barsoum et al., 2003; Barsoum and Radovic, 2011; Plummer et al., 2021; Rathod et al., 2021). In these anisotropic layered materials, such as fiber-reinforced composites (and to some extent, MAX phases), the formation of kinkbands under compression parallel to the layers involves three stages: First, the relatively stiffer layers (fibers in composites or MX layers in MAX phases) undergo micro-buckling ((Moran et al., 1995; Plummer et al., 2021; Rosen, 1970). Second, post-buckling deformation localizes into a well-defined band, which serves as the prelude to the kink-band (Hsu et al., 1998; Kyriakides et al., 1995; Vogler et al., 2001; Vogler and Kyriakides, 2001). Finally, the inclination, width or both of the kink-band increase with progressive deformation (Hsu et al., 1998; Kyriakides et al., 1995; Vogler et al., 2001; Vogler and Kyriakides, 2001).

A key ingredient in the formation of kink-bands in almost all susceptible materials is anisotropic deformation. In the case of bimetallic layered composites, it has been proposed that the presence of ultrathin layers restricts the accumulation of dislocations, and plastic deformation primarily occurs through the movement of dislocations parallel to the layers, resulting in plastic anisotropy. This phenomenon is known as confined layer slip (Anderson et al., 1999; Jian et al., 2022; Misra et al., 2005; Subedi et al., 2018; Wang and Misra, 2014). However, the initiation of kink-bands in

bimetallic layered composites is believed to differ from other susceptible materials. This is because, unlike the latter, the former does not possess stiff or rigid layers, and all layers can undergo elastic-plastic deformation (Nizolek et al., 2015). Additionally, the strain fields surrounding a kink-band in bimetallic layered composites have been found to resemble an inclined crack with mixed Mode-I and Mode-II components (Nizolek et al., 2017). Furthermore, a detailed post-mortem analysis of kink-bands in Cu-Nb bimetallic layered composites revealed significant changes in the microstructure of these materials (Zhang et al., 2022). This includes the accumulation of geometrically necessary dislocations and the presence of tilt geometrically necessary boundaries near the boundaries of the kink-band.

Nevertheless, it is reasonable to assume that the onset of kink-band formation, even in bimetallic layered composites, requires some sort of instability. Additionally, the formation and overall morphology of the kink-bands in these materials may not be strongly influenced by the details of the layer-level microstructure and/or deformation mechanisms. Instead, the layer-level initial microstructural details, in conjunction with their unique deformation mechanism, only drive the distinct microstructure evolution within the kink-bands.

Herein, we propose a hypothesis that layer refinement, together with the strength differential between the layers of the two materials, alone constitutes 'sufficient conditions' to trigger kink-banding in bimetallic layered composites. That is, considering elastically stiff layers, geometrical imperfections (such as waviness of the layers), and extreme plastic anisotropy within the layers may not be the 'necessary conditions' for the occurrence of kink-banding in these composites. Note that in our hypothesis, plastic anisotropy within the layers is not assumed to be a 'necessary

condition.' However, it is important to acknowledge that the strength differential between the layers of the two materials will inherently introduce anisotropy in the response of the composite material. To prove our hypothesis, we carried out extensive plane strain finite element finite deformation analyses of bimetallic layered composites subjected to layer parallel compression. Additionally, we carried out limited analyses of the same under layer normal compression. In the calculations, both constituent materials were assumed to follow a rate-independent isotropic elastic-plastic constitutive relation with an ad-hoc thickness dependent yield strength.

Aligned with our hypothesis, the results demonstrate that when bimetallic layered composites are subjected to layer parallel compression, layer refinement and the associated Hall-Petch strengthening-induced increase in the difference between the strength of the constituent materials naturally capture the transition in the mode of deformation from barreling to kink-band formation. These factors also naturally capture the formation of shear-bands in these composite materials when subjected to layer normal compression, as in the experiments (Snel et al., 2017). Furthermore, we conducted parametric studies to understand the individual effects of layer thickness, strength differential between the two constituent materials, and strain-hardenability of the materials on kink-band formation. The results of our parametric studies show that the strain-hardenability of the constituent materials in bimetallic layered composites stabilizes the formation of kink-bands. Importantly, it leads to a transition from the abrupt formation of through-width kink-bands to the onset and propagation of stable inclined wedge-shaped kink-bands, as observed in the experiments of Nizolek et al. (2015).

Recently, three other works have addressed kink-band formation in bimetallic layered composites. Each primarily aimed to showcase the capabilities of its respective methodology. Zecevic et al. (2022) employed a large-strain elasto-viscoplastic formulation based on fast Fourier transforms. In a follow-up, Zecevic et al. (2023) adopted a non-local version of this method. Meanwhile, Arora et al. (2023) employed finite deformation mesoscale field dislocation mechanics. All three works focused on modeling kink-band formation in Cu-Nb bimetallic composite materials, drawing from observations in small-scale micropillar compression tests by Nizolek (2016) and Zhang et al. (2022). While these works, notably that of Zecevic et al. (2023), qualitatively captured various facets of microstructural evolution within the kink-bands observed in the small-scale experiments, our work seeks to understand and rationalize kink-band formation in larger-scale specimens (on the order of few millimeters) as observed in the experiments of Nizolek et al. (2015).

#### 2. Numerical method

We have carried out micromechanical analyses of bimetallic layered composite specimens subjected to layer parallel compression as shown in **Fig. 1** using plane strain finite element finite deformation calculations. All the finite element calculations are carried out using the commercial finite element code ABAQUS/Standard. The overall in-plane dimensions, height (h) and width (w) of the specimens modeled are 7.2  $\mu$ m and 3.6  $\mu$ m, respectively, giving an aspect ratio (h/w) of 2 which is the same as in the experiments of Nizolek et al. (Nizolek et al., 2017; Nizolek et al., 2015). The specimens modeled contain alternating layers of the same thickness, t, of two materials referred to as Material 1 and Material 2. The layers in the finite element models are assumed to be initially straight and remain completely bonded as no interlayer decohesion was observed in the

experiments (Nizolek et al., 2015). As shown schematically in **Fig. 1**, the specimen is supported on a rigid support while being compressed using a rigid punch.

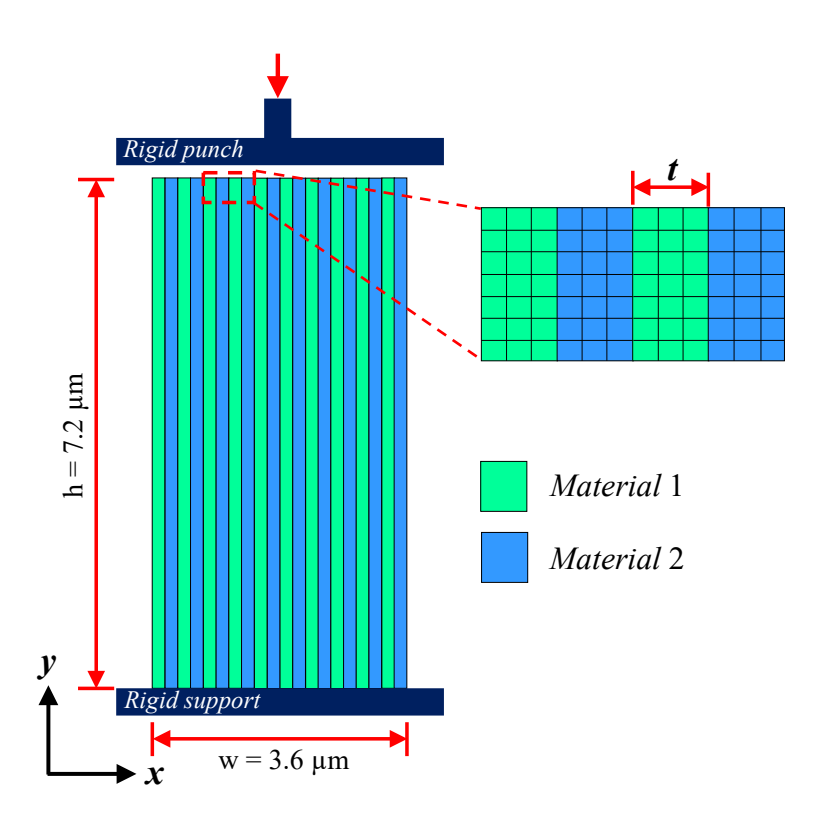


**Figure 1.** Schematic representation of plane strain finite element model of a bimetallic layered composite (composed of layers of material 1 and 2 of thickness, t) specimen which is supported at the bottom using a rigid support while being compressed from the top using a rigid punch.

The finite element mesh for the specimens is generated using eight-node quadratic plane strain elements with at least three elements through the thickness of individual layers, while the rigid support and punch are modeled using two-node plane strain rigid elements. A surface-surface contact with a coefficient of friction 0.1 is invoked between the top and bottom surfaces of the specimen and the rigid punch and support, respectively. At the beginning of the calculations, the top and bottom surfaces of the specimens are taken to be in direct contact with the rigid punch and

support, respectively. The x and y displacements of the rigid support, and x displacement of the rigid punch are constrained throughout the calculation and the rigid punch is displaced along the -y direction to impose compressive deformation on the specimen. Both Material 1 and Material 2 are modeled as rate-independent isotropic elastic-plastic material within finite strain  $J_2$  flow theory. For both the materials the linear elastic response is characterized by the Young's modulus (E) and Poisson's ratio (v), and the plastic response is modeled as,

$$\sigma = \sigma_y \left[ 1 + K \left( \bar{\varepsilon}_{pl} \right)^n \right] \tag{1}$$

where,  $\sigma$  is the flow stress,  $\sigma_y$  is the yield strength of the material,  $\bar{\varepsilon}_{pl}$  is the effective plastic strain, K is the strain-hardening coefficient, and n is the strain-hardening exponent.

Since the objective of our micromechanical analyses is to understand the onset and evolution of instabilities, specifically kink-bands, in bimetallic layered composite materials, it is necessary to introduce some sort of perturbation in the analyses. Analyzing a perfect system alone would essentially be a bifurcation problem and would result in significantly higher load/deformation levels for the onset of any instability (Nestorović and Triantafyllidis, 2004; Triantafyllidis and Maker, 1985). In the case of fiber-reinforced composites, a small imperfection such as fiber misalignment is typically introduced to study kink-band formation (Argon, 2013; Budiansky, 1983; Kyriakides et al., 1995; Vogler et al., 2001). In our calculations, we introduced a small imperfection by randomly perturbing the values of  $\sigma_y$  for individual layers of materials 1 and 2 by  $\pm 1\%$ . Additionally, we analyzed cases where a small tilt of 1° was introduced at the interfaces between the layers of materials 1 and 2.

Supplementary Figure S1 contrasts the effects of material and geometric perturbations on the response of bimetallic layered composite specimens under layer-parallel compression. This figure further delineates the impact of these perturbations for specimens with two different aspect ratios. As illustrated in the figure, the value of imposed nominal compressive strain at the drop in the load-carrying capacity of the specimen with an aspect ratio of 2 with a geometrical perturbation is approximately 7% less than that with a material perturbation. For the specimen with an aspect ratio of 4, the difference increases to approximately 12%. It's crucial to underscore that in bimetallic layered composites, geometrical perturbations correspond to the waviness of the layers (Carpenter et al., 2014). However, our primary objective is to highlight that the presence of layer waviness is not a 'necessary condition' for kink-banding in these materials. Consequently, in all subsequent analyses presented, only material perturbation is considered.

#### 3. Numerical results

Our objective is to rationalize the effects of structural and material parameters on the onset of kink-band formation in bimetallic layered composites observed in the experiments of Nizolek et al. (Nizolek et al., 2017; Nizolek et al., 2015). In these experiments, it was observed that the propensity of kink-band formation under layer parallel compression in Cu-Nb bimetallic layered composites increases with increasing layer refinement (i.e., decreasing layer thickness or increasing the number of layers within a fixed sized specimen). Following this, we first analyze the concomitant effect of layer refinement and associated Hall-Petch strengthening (Hall, 1951; Petch, 1953) on the onset of kink-band formation in Section 3.1. Next, we analyze the individual

effects of layer thickness and strength differential between the two constituent materials in Section 3.2. Finally, parametric studies are carried out to analyze the effects of strain-hardenability of the materials on the onset of kink-band formation in Section 3.3.

#### 3.1 Concomitant effect of layer refinement and Hall-Petch strengthening

In nanoscale bimetallic layered composites, the layer thickness and dislocation distributions play important roles in dislocation motion (Jian et al., 2022) and even though dislocation pileups may not be expected in fine nanolayered structures, dislocation density accumulation at the interfaces (Subedi et al., 2018) or dislocation emission from the interfaces (Chen et al., 2020) give rise to Hall-Petch type strengthening in these materials. An increase in the yield strength of the Cu-Nb bimetallic composites with decreasing layer thickness has been experimentally observed under both layer parallel (Nizolek et al., 2015) and normal compressions (Snel et al., 2017), as well as during indentation (Misra et al., 2005), at least for layer thicknesses up to a few tens of nanometers. However, a separate characterization of the effect of layer thickness on the yield strength of the two constituent materials in the composite is currently unavailable. Following this, we assume that the value of  $\sigma_y$  in Eq. (1) for both the materials in the bimetallic layered composites follows Hall-Petch strengthening (Hall, 1951; Petch, 1953) which relates  $\sigma_y$  to layer thickness, t, as

$$\sigma_{y} = \sigma_{o} + k \left(\frac{1}{\sqrt{t}}\right) \tag{2}$$

where,  $\sigma_o$  and k are material parameters. The values of  $\sigma_0$  and k for material 1 (Cu) are taken to be 40 MPa and 110 MPa $\sqrt{\mu m}$ , respectively, while for material 2 (Nb), they are taken to be 120

MPa and 340 MPa $\sqrt{\mu m}$ , respectively, following Cordero et al. (2016), where these values were obtained for bulk Cu and Nb. For these values of  $\sigma_o$  and k, not only the strength of the two materials in the composite increases with decreasing layer thickness but the difference between their strength also increases with decreasing layer thickness. For example, for t = 360 nm, the strength difference between materials 2 and 1 is approximately 470 MPa, while for t = 30 nm, the difference is around 1300 MPa. However, in relative terms, they are fairly similar. The strength of Material 2 relative to Material 1 is approximately 3 for both t = 360 nm and t = 30 nm. The values of E and  $\nu$  for material 1 are taken to be 110 GPa and 0.34, respectively, while for material 2 are taken to be 103 GPa and 0.38, respectively. The values of the strain-hardening parameters, E and E and E are taken to be 0.1 and 0.3, respectively, for both the materials.

The calculated nominal compressive stress-strain response of four bimetallic layered composite specimens with layer thickness 360 nm, 90 nm, 60 nm and 30 nm is shown in Fig. 2(a). As shown in the figure, at the early stages of deformation, all specimens exhibit a linear stress-strain response which is followed by a slight change in the slope of the curve, Fig. 2(b). This slight change in the slope of the stress-strain curve corresponds to the yielding of the softer material (material 1), and since the yield strength of the softer material follows Hall-Petch strengthening, the stress at which the slope changes increases with decreasing layer thickness. Next, with continued deformation, all the specimens undergo macroscopic yielding marked by the onset of non-linearity in the stress-strain response, and since the yield strength of the harder material (material 2) also follows Hall-Petch strengthening, the stress at the onset of non-linearity increases with decreasing layer thickness. The increase in the stress at macroscopic yielding with decreasing layer thickness, as shown in Fig. 2, is consistent with the experimental results of both layer normal (Snel et al., 2017)

and layer parallel compression (Nizolek et al., 2015) of Cu-Nb bimetallic layered composite materials. Finally, after a finite amount of deformation following macroscopic yielding, the stress carrying capacity of three specimens with layer thickness,  $t \le 90$  nm, first decreases and then tends to saturate. The imposed nominal compressive strain at the onset of the decrease in the stress carrying capacity of the specimens decreases; while the extent and the rate of decrease (with respect to the nominal strain) of the same increases with decreasing layer thickness.

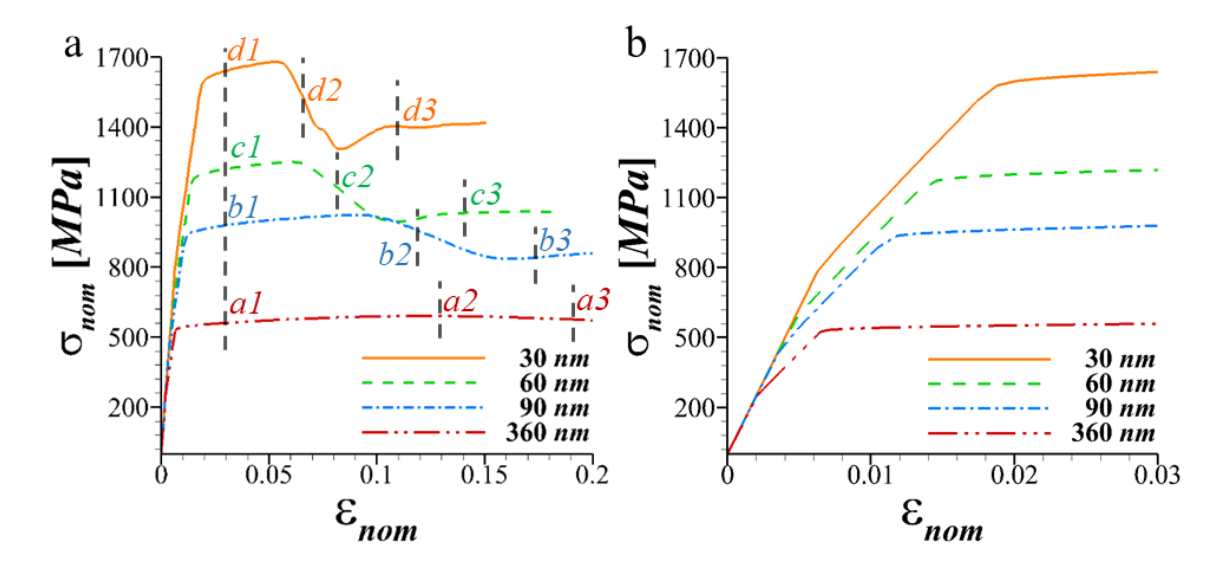


**Figure 2.** (a) Nominal compressive stress-strain response of bimetallic layered composite specimens with different layer thicknesses and thickness-dependent yield strength. (b) Early stage nominal compressive stress-strain response of bimetallic layered composite specimens shown in (a).

The variation of the effective plastic strain,  $\bar{\varepsilon}_{pl}$ , in the four bimetallic layered composite specimens at three levels of imposed nominal compressive strain is shown in Fig. 3. As shown in Fig. 3(a1-a3), the specimen with layer thickness 360 nm that did not exhibit a decrease in the stress carrying capacity post macroscopic yielding in Fig. 2(a), predominantly deforms in a barrel-like fashion. Next, with continued deformation, the effective plastic strain in this specimen localizes in two

intersecting bands that are roughly inclined at  $\pm 45^{\circ}$  with respect to the compression axis. The other three specimens with layer thickness 90 nm and below, also at least initially deform in a barrel-like fashion, Fig. 3(b1-d1), but with continued deformation, the free edges of the deformed specimens take a double taper shape, Fig. 3(b3-d3). The two tapers on both the free edges of these specimens are at the locations where the bands of extremely localized plastic deformation intersect with the free edges. Similar to the specimen with 360 nm thick layers, the localized plastic deformation bands in the specimens with layer thickness 90 nm and below are also roughly inclined at  $\pm 45^{\circ}$  with respect to the compression axis. However, the extent of plastic deformation within the bands in these specimens is much greater than the specimen with layer thickness 360 nm, even at significantly lower levels of the imposed nominal compressive strains.

A careful examination of deformation in the bands shows that unlike the specimen with layer thickness 360 nm, the microstructure within the bands in specimens with layer thickness 90 nm and below are significantly misoriented compared to the regions outside the band (see inserts a2-a3 and d2-d3 in Fig. 3). Thus, the localized plastic deformation bands in all the specimens with layer thickness 90 nm and below are essentially kink-bands with in-plane rotation,  $\alpha$ , of the material (layers) inside the kink-band being roughly twice that of the inclination of the kink-band boundaries,  $\beta$ , so that the nominal volumetric strain (Dewey, 1965),  $\Delta V/V = \cos(\beta - \alpha) \sec(\beta) - 1$ , inside the kink-band is zero. Moreover, decreasing the layer thickness in the specimens not only promotes early kink-band formation (i.e., a decrease in the imposed nominal compressive strain at the onset of kink-band formation) but also results in finer kink-bands. Finally, post kink-band formation (i.e., post decrease in the stress carrying capacity) the specimens with layer thickness 90 nm and below deform by kink-band widening at roughly constant nominal

stress, see Figs. 2(a) and 3(b2-d3). The regime in which the kink-band widens while the nominal stress carrying capacity of the specimens remains relatively constant can be seen more clearly in the Supplementary Movie S1.

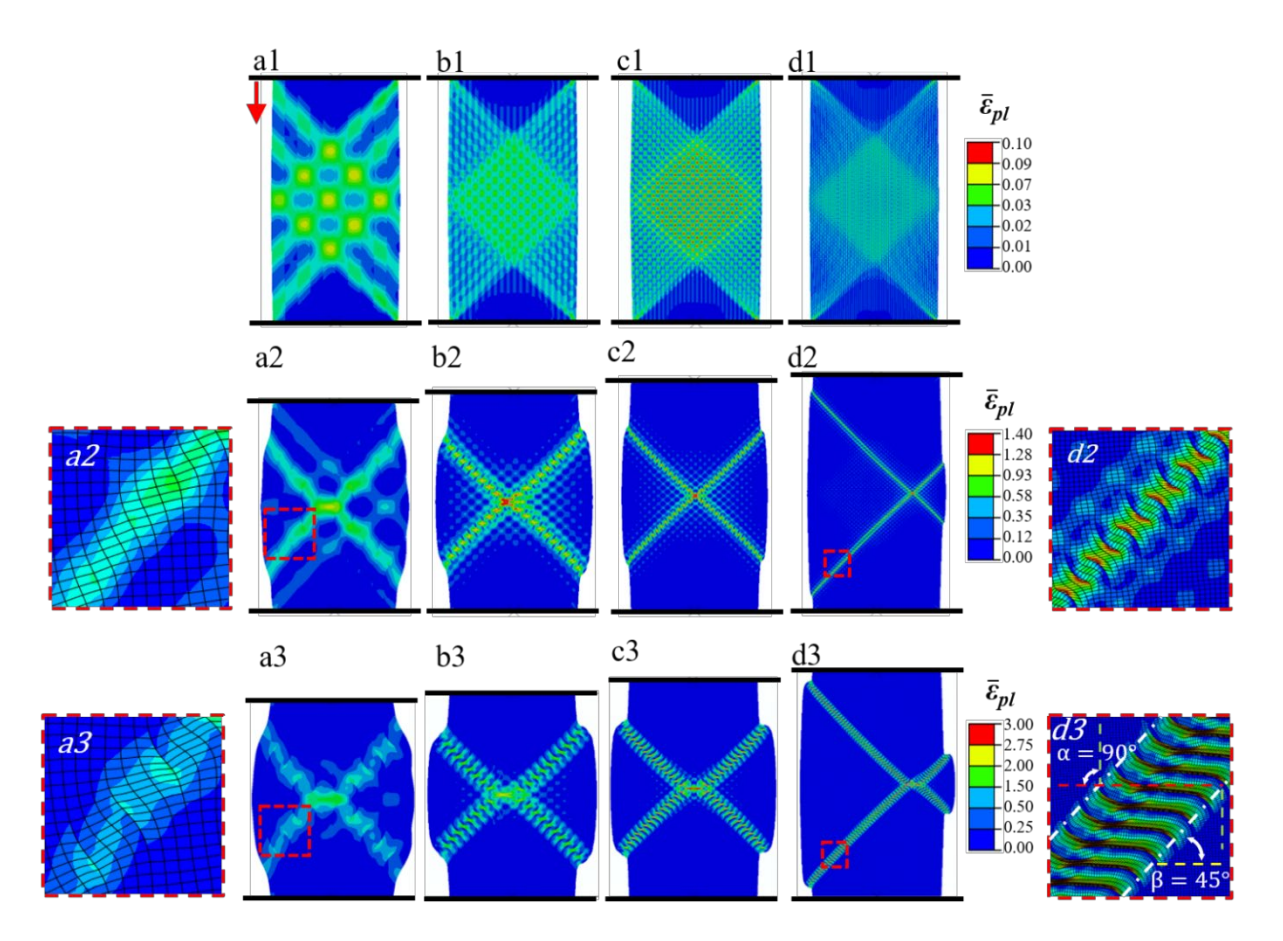


Figure 3. Contour plots of the effective plastic strain,  $\bar{\varepsilon}_{pl}$ , in bimetallic layered composite specimens with different layer thicknesses and thickness-dependent yield strength at three imposed nominal compressive strain levels. The contour plots a1-a3, b1-b3, c1-c3 and d1-d3 correspond to the specimens with layer thickness 360 nm, 90 nm, 60 nm and 30 nm, respectively. The respective imposed nominal compressive strain levels for all the contour plots are marked with dashed vertical lines on the stress-strain curves shown in Fig. 2(a). The left inserts show the zoomed view of the regions marked with dashed boxes in the contour plots a2 and a3, while the right inserts show the zoomed view of the regions marked with dashed boxes in the contour plots d2 and d3.

## 3.2 Effects of layer thickness and strength differential

The results presented in Section 3.1 show the concomitant effect of both layer refinement and Hall-Petch strengthening induced increase in the difference between the strength of the two materials with decreasing layer thickness on the formation of kink-bands in bimetallic layered composites. In this section, we focus on the individual effect of layer thickness and the difference between the strength of the two materials. To this end, we first analyze the effect of layer thickness by assuming that the value of  $\sigma_y$  in Eq. (1) for the two materials is independent of their layer thickness and are taken to be 500 MPa and 1500 MPa for materials 1 and 2, respectively; while the values of other parameters, E, v, K and n, are taken to be the same as in Section 3.1.

The calculated nominal compressive stress-strain response of four bimetallic layered composite specimens with layer thickness 360 nm, 90 nm, 60 nm and 30 nm but with thickness-independent properties is shown in Fig. 4. As shown in the figure, at the early stages of deformation, all specimens exhibit a linear stress-strain response which is followed by a small change in the slope of the curve. This change in slope of the stress-strain curve corresponds to the yielding of the softer material (material 1), and since the yield strength of the softer material is independent of the layer thickness, the stress at which the slope changes is the same for all the specimens. Next, with continued deformation, all the specimens undergo macroscopic yielding marked by the onset of non-linearity in the stress-strain response, and again since the yield strength of the harder material (material 2) is also independent of the layer thickness, the stress at the onset of non-linearity is the same for all the specimens. Following the onset of non-linearity and after a finite amount of

deformation, the stress carrying capacity of the three specimens with layer thickness,  $t \le 90$  nm, first decreases and then tends to saturate. As discussed in Section 3.1, the decrease in the stress carrying capacity of the specimens corresponds to the formation of kink-bands. The imposed nominal compressive strain at the onset of the decrease in the stress carrying capacity of the specimens decreases while the rate of decrease of the stress carrying capacity of the specimens increases with decreasing layer thickness. However, unlike the results presented in Fig. 2, the extent of decrease in the stress carrying capacity in Fig. 4 for  $t \le 90$  nm post kink-band formation is not significantly affected by decreasing layer thickness when the strength of the two materials are taken to be independent of the layer thickness.

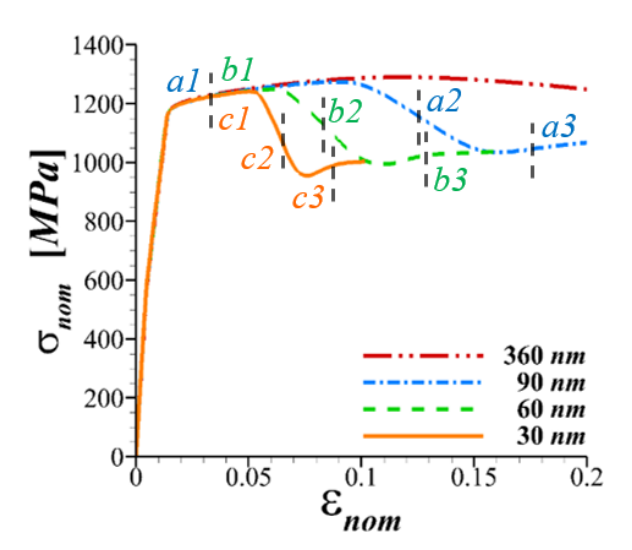


**Figure 4.** Nominal compressive stress-strain response of bimetallic layered composite specimens with different layer thickness but with thickness-independent yield strength.

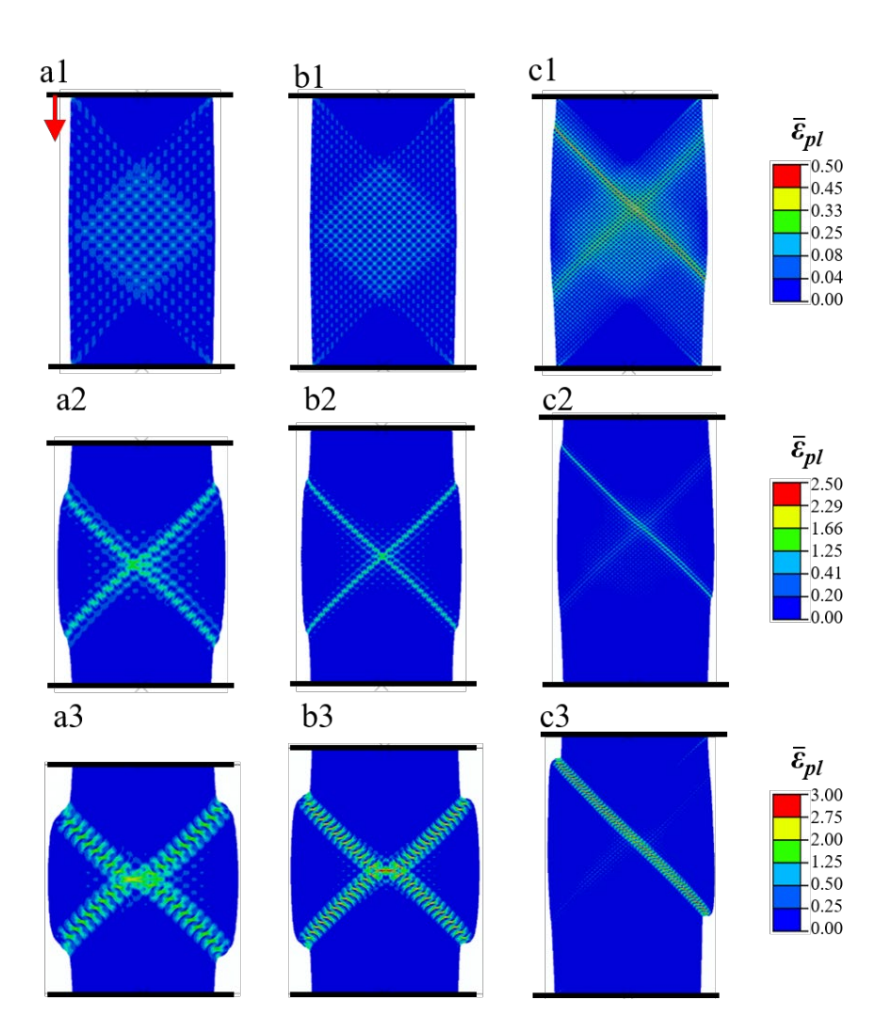


**Figure 5.** Contour plots of the effective plastic strain,  $\bar{\varepsilon}_{pl}$ , in bimetallic layered composite specimens with different layer thicknesses and thickness-independent yield strength at three imposed nominal compressive strain levels. The contour plots a1-a3, b1-b3 and c1-c3 correspond to the specimens with layer thickness 90 nm, 60 nm and 30 nm, respectively. The respective imposed nominal compressive strain levels for all the contour plots are marked with dashed vertical lines on the stress-strain curves shown in Fig. 4.

The variation of the effective plastic strain,  $\bar{\varepsilon}_{pl}$ , in the three bimetallic layered composite specimens that exhibit a decrease in the stress carrying capacity following the onset of non-linearity, Fig. 4, at three levels of imposed nominal compressive strain are shown in Fig. 5. As shown in the figure, all three specimens at least initially deform in a barrel-like fashion but with

continued deformation, these specimens deform by kink-band formation and kink-band widening. Although for these three specimens the material properties are taken to be independent of the layer thickness, decreasing the layer thickness in the specimens promotes the early onset of kink-band formation (i.e., decrease in the imposed nominal compressive strain at the onset of kink-band formation) as well as the formation of finer kink-bands. Note that even though the specimen with layer thickness 30 nm initially shows signs of two intersecting bands of effective plastic strain, only one of them eventually evolves into a kink-band in this specimen, Fig. 5(c1-c3). The intersecting kink-bands in Figs. 5(a2-a3) and (b2-b3), and one in Fig. 5(c2-c3) are roughly inclined at angles of  $\pm 50^{\circ}$  and  $-50^{\circ}$ , respectively, with respect to the compression axis.

We now analyze the effect of the difference between the strength of the two materials by considering a specimen with a fixed layer thickness of 30 nm. In this set of calculations, the value of  $\sigma_y$  in Eq. (1) for material 1 is fixed to 500 MPa and that of material 2 is assumed to be either 500 MPa, 1000 MPa, 1500 MPa or 2000 MPa; while the values of other parameters, E,  $\nu$ , K and n, are taken to be the same as in Section 3.1.

The calculated nominal compressive stress-strain response of bimetallic layered composite specimens with layer thickness 30 nm but different values of  $\sigma_y$  for material 2 is shown in Fig. 6. As shown in the figure, the specimen with  $\sigma_y$  being 500 MPa for both the materials first exhibits linear stress-strain response which is followed by the onset of macroscopic yielding. All other specimens also first exhibit linear stress-strain response which is followed by a slight change in the slope of the curve due to early yielding in material 1 before the onset of macroscopic yielding. The onset of macroscopic yielding in these specimens occur at increasing nominal stress levels

consistent with the increase in the value of  $\sigma_y$  for material 2. Following the onset of macroscopic yielding and after a finite amount of deformation, the stress carrying capacity of the specimens with  $\sigma_y \geq 1000$  MPa for the material 2, first decreases and then tends to saturate. Here as well, the decrease in the stress carrying capacity of the specimens corresponds to the formation of kinkbands and the nominal strain at the onset of the decrease in the stress carrying capacity decreases while the rate of decrease of the stress carrying capacity increases with increasing value of  $\sigma_y$  for material 2 (i.e., the increasing difference between the strength of the two materials in the bimetallic layered composite specimens with a fixed layer thickness). Also, similar to the results presented in Fig. 2 (but unlike the results presented in Fig. 4), the extent of decrease in the stress carrying capacity in Fig. 6 for  $\sigma_y \geq 1000$  for material 2, increases with increasing difference between the strength of the two materials in the composite specimens.

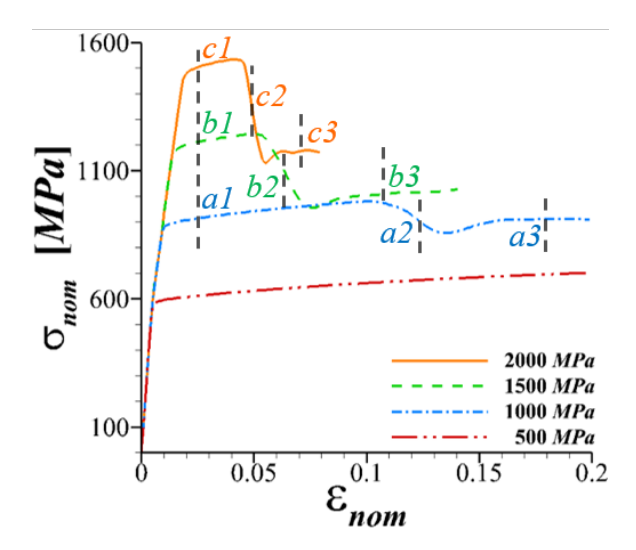


**Figure 6.** Nominal compressive stress-strain response of bimetallic layered composite specimens with a fixed layer thickness of 30 nm and the yield strength of material 1 being fixed to 500 MPa while that of material 2 being either 500 MPa, 1000 MPa, 1500 MPa or 2000 MPa.

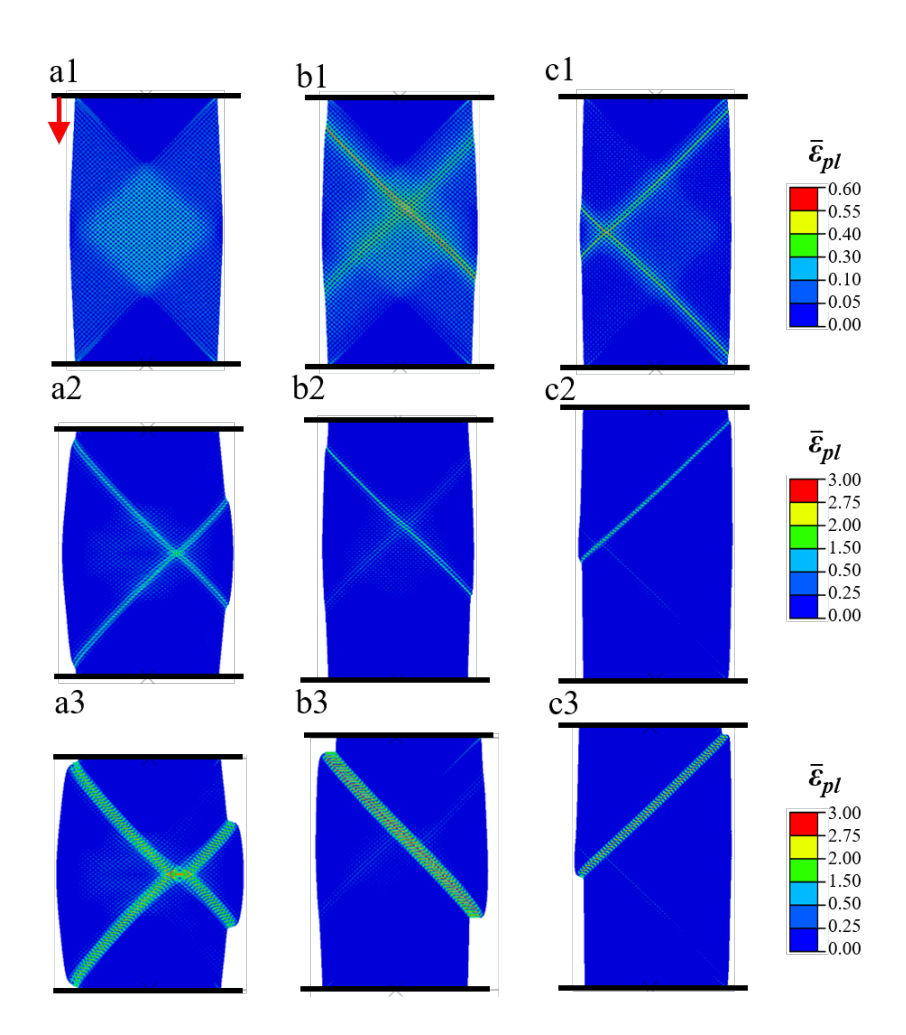


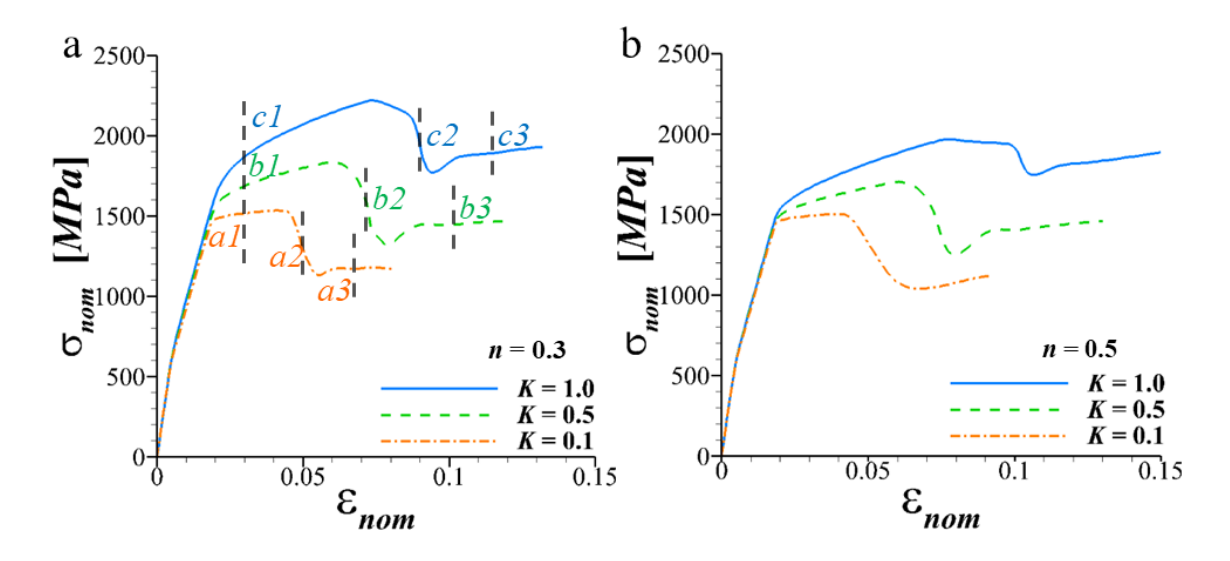
Figure 7. Contour plots of the effective plastic strain,  $\bar{\varepsilon}_{pl}$ , in bimetallic layered composite specimens with a fixed layer thickness of 30 nm but three values of the yield strength of material 2 at three imposed nominal compressive strain levels. The contour plots a1-a3, b1-b3 and c1-c3 correspond to the specimens wherein the yield strength of material 1 is fixed to 500 MPa while that of material 2 is taken to be either 1000 MPa, 1500 MPa or 2000 MPa, respectively. The respective imposed nominal compressive strain levels for all the contour plots are marked with dashed vertical lines on the stress-strain curves shown in Fig. 6.

Figure 7 shows the variation of the effective plastic strain,  $\bar{\varepsilon}_{pl}$ , at three levels of imposed nominal compressive strain in the bimetallic layered composite specimens with layer thickness 30 nm and  $\sigma_y = 1000$  MPa, 1500 MPa and 2000 MPa for material 2. All of these three specimens with

 $\sigma_y \ge 1000$  MPa for material 2 show decrease in the stress carrying capacity following the onset of macroscopic yielding (see Fig. 6). As shown in Fig. 7, these specimens at least initially deform in a barrel-like fashion but with continued deformation these specimens deform by kink-band formation and kink-band widening. Although in all these three specimens the layer thickness is the same, increasing the value of  $\sigma_y$  for material 2 (i.e., increasing the difference between the strength of the two materials) in the bimetallic layered composite not only promotes the early onset of kink-band formation but also results in the formation of finer kink-bands. Similar to Fig. 5, in Fig. 7 as well, even though the specimens with  $\sigma_y \ge 1500$  MPa for material 2 initially show signs of two intersecting bands of effective plastic strain, only one of them finally evolves into a kink-band in these specimens. The intersecting kink-bands in Fig. 7(a2-a3), and one in Fig. 7(b2-b3) are roughly inclined at angles of  $\pm 45^\circ$  and  $\pm 45^\circ$ , respectively, while one in Fig. 7(c2-c3) is roughly inclined at an angle of  $\pm 50^\circ$  with respect to the compression axis.

#### 3.3 Effect of strain-hardening parameters

In this section, we focus on analyzing the effect of materials' strain-hardenability characterized by the values of the parameters, K and n in Eq. (1) on the formation of kink-bands. To this end, we consider a specimen with a layer thickness of 30 nm and the value of  $\sigma_y$  being 500 MPa for material 1 and 2000 MPa for material 2; while the values of the elastic constants E and v are taken to be the same as in Section 3.1.



**Figure 8.** Nominal compressive stress-strain response of bimetallic layered composite specimens with a fixed layer thickness of 30 nm and fixed values of the yield strength, 500 MPa and 2000 MPa, for materials 1 and 2, respectively, but with three values of the strain-hardening coefficient, K, and two values of the strain-hardening exponent, (a) n = 0.3 and (b) 0.5, for both the materials.

Figure 8 shows the effect of strain-hardenability of the material on the nominal compressive stress-strain response of bimetallic layered composite specimens. The results are shown for the values of n = 0.3 and 0.5, and for each value of n, the results are shown for values of K = 0.1, 0.5 and 1.0, taken to be the same for both the materials in the composite specimens. As expected, at the early stages of deformation all specimens exhibit linear stress-strain response which is followed by a small change in the slope of the curve and with continued deformation, all the specimens undergo macroscopic yielding. Since the yield strength of both the materials in all three specimens is fixed, the change in slope of the curves, as well as the macroscopic yielding, occurs roughly at the same imposed nominal compressive strain levels. However, post macroscopic yielding the stress-strain response of the specimens strongly depends on the value of K, while for a fixed value of K the difference between the stress-strain response for n = 0.3, Fig. 8(a), and 0.5, Fig. 8(b), is rather

small. As shown in Fig. 8, with increasing value of K, the stress-strain response of the specimens exhibits an increase in the level of strain-hardening as well as an increase in the imposed nominal compressive strain at the onset of the decrease in the stress carrying capacity of the specimens post macroscopic yielding.

The variation of the effective plastic strain,  $\bar{\varepsilon}_{pl}$ , in the three bimetallic layered composite specimens wherein the value of n is taken to be 0.3 and that of K is taken to be either 0.1, 0.5 or 1.0 for both the materials at three levels of imposed nominal compressive strain are shown in Fig. 9. As shown in the figure, all three specimens initially tend to deform in a barrel-like fashion but with continued deformation, these specimens deform by kink-band formation. The specimen in Figs. 9(a1-a3), with K = 0.1, exhibits post barreling deformation characterized by the abrupt formation of a single fine kink-band spanning the entire width of the specimen. This kink-band then undergoes stable widening at a roughly constant nominal stress. However, for specimens with  $K \ge 0.5$ , as shown in Figs. 9(b1-c3), the post barreling deformation occurs through the onset and propagation of two relatively thick wedge-shaped kink-bands. These wedge-shaped kink-bands originate from the two corners of the specimens and gradually expand across the width of the specimen with progressive deformation. During this growth process, both the inclination and width of the kink-bands tend to increase. In Fig. 9(a3), the single kink-band in the specimen with K = 0.1has a rough inclination of approximately 50°, while in Figs. 9(b3) and (c3), the two wedge-shaped kink-bands in the specimens with K = 0.5 and 1.0 are roughly inclined at  $\pm 60^{\circ}$  and  $\pm 65^{\circ}$ , respectively, with respect to the compression axis. The formation and propagation of the wedgeshaped kink-bands in Figs. 9(b1-b3) and (c1-c3) closely resemble those observed experimentally in Cu-Nb bimetallic layered composites by Nizolek et al. (2015).

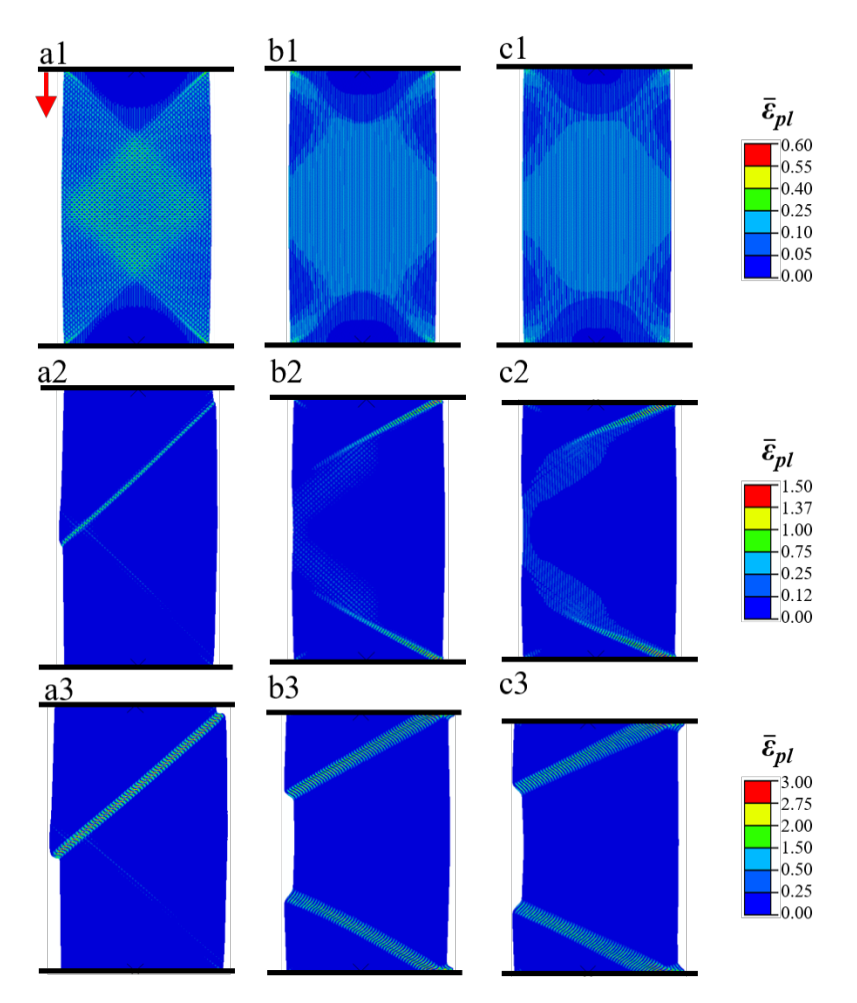


Figure 9. Contour plots of the effective plastic strain,  $\bar{\epsilon}_{pl}$ , in bimetallic layered composite specimens with a fixed layer thickness of 30 nm and fixed values of the yield strength, 500 MPa and 2000 MPa, for materials 1 and 2, respectively, but for three values of the strain-hardening coefficient, K, and one value of the strain-hardening exponent, n = 0.3, at three imposed nominal compressive strain levels. The contour plots a1-a3, b1-b3 and c1-c3 correspond to the specimens wherein the values of the strain-hardening coefficient are taken to be 0.1, 0.5 and 1.0, respectively, for both the materials. The respective imposed nominal compressive strain levels for all the contour plots are marked with dashed vertical lines on the stress-strain curves shown in Fig. 8.

#### 4. Discussion

The motivation for our work stems from the experimental observation of kink-band formation in Cu-Nb bimetallic layered composites (Nizolek et al., 2017; Nizolek et al., 2015). In the experiments, it was observed that under layer parallel compression, the mode of deformation of Cu-Nb bimetallic layered composites changes from barreling to kink-band formation with increasing layer refinement (i.e., decreasing layer thickness or increasing the number of layers within a fixed sized specimen). To rationalize the experimental observations, we carried out micromechanical analyses of deformation and instability in bimetallic layered composite specimens subjected to layer parallel compression using plane strain finite element finite deformation calculations. In the calculations, both the materials are assumed to follow rate-independent isotropic elastic-plastic constitutive relation with an ad-hoc thickness dependent yield strength.

Our results demonstrate that in line with our initial hypothesis, layer refinement, along with the strength differential between the layers of the constituent materials, naturally captures the transition in the mode of deformation from barreling to kink-band formation. Thus, the presence of elastically stiff layers, geometric imperfections (such as layer waviness), and extreme plastic anisotropy within the layers are not the necessary conditions for the occurrence of kink-banding in these composite materials. We note that although we did not consider plastic anisotropy within the layers, the strength differential between the constituent materials inherently introduces anisotropy in the response of the composite material. Furthermore, other experimental observations naturally emerged in our finite element calculations, including (i) an increase in the

strength of the composite material, (ii) an enhanced propensity for kink-band formation, and (iii) the formation of finer kink-bands as the layer thickness decreases.

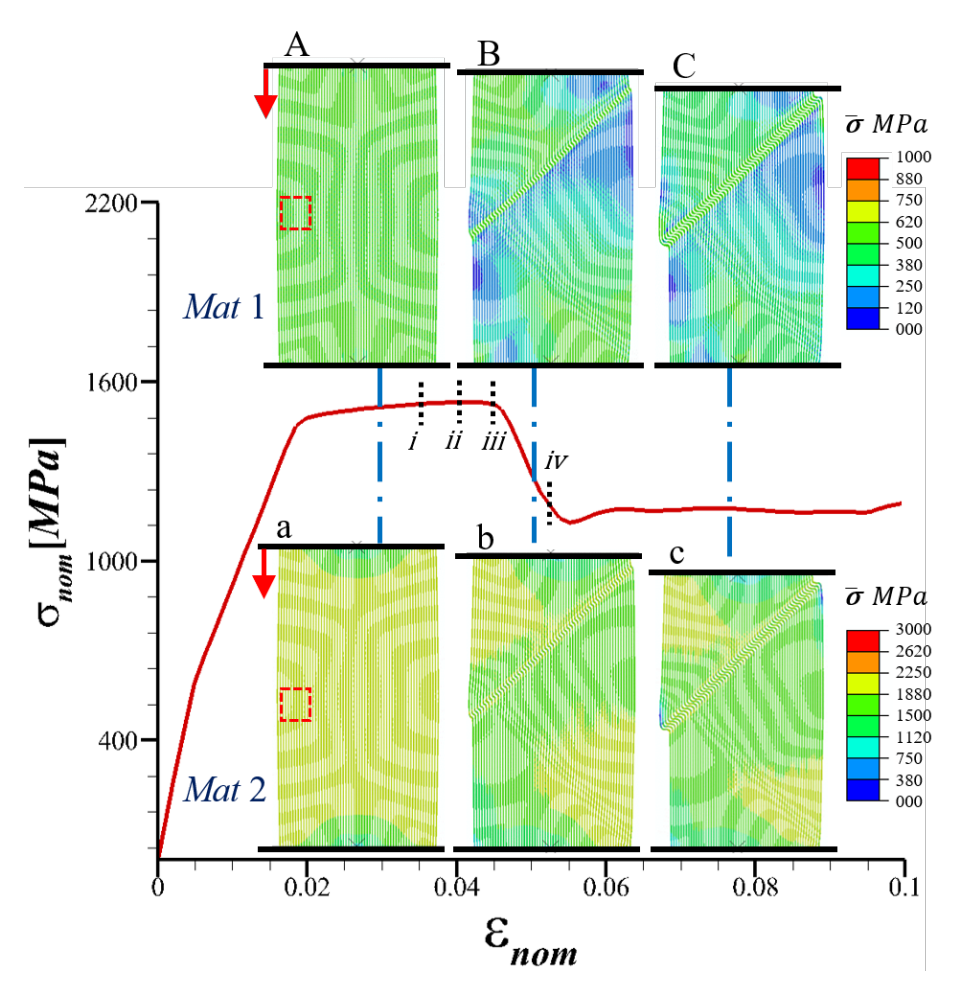


**Figure 10.** Nominal compressive stress-strain response of a bimetallic layered composite specimen with a layer thickness of 30 nm, yield strength of 500 MPa and 2000 MPa for materials 1 and 2, respectively, and strain-hardening coefficient and exponent, 0.1 and 0.3, respectively for both the materials. The distribution of effective stress,  $\bar{\sigma}$ , in the layers of material 1 at three imposed nominal compressive strain levels are shown in the top row (A-C) and the same in the layers of material 2 are shown in the bottom row (a-c).

To elucidate the effect and the mechanism of kink-band formation in bimetallic layered composite specimens, we analyzed the evolution of effective stress, Fig. 10, and plastic strain, Fig. 11, in the individual layers of the two materials. The results in Figs. 10 and 11 are for a specimen with a layer thickness of 30 nm. The values of  $\sigma_v$  for materials 1 and 2 are taken to be 500 MPa and 2000 MPa, respectively, while the values of all other parameters are the same as in Section 3.1. As shown in Figs. 10(A) and (a), following the macroscopic yielding the level of effective stress in the layers of (softer) material 1 is less than that of the layers of (harder) material 2. This is expected as the composite is nominally subjected to iso-strain compression. However, as shown in Fig. 11, the distribution of effective plastic strain in the individual layers of the two materials in a small region (marked with a dashed box in Figs. 10A and a) which is eventually engulfed by the kinkband in the specimen is remarkably distinct even before the onset of any macroscopic instability. The distribution of plastic strain in the layers of the softer material is discrete, Fig. 11(a), while in the layers of the harder material is wavy, Fig. 11(b), at an imposed nominal strain level marked 'i' on the stress-strain curve in Fig. 10. It is important to note that the size and spacing of the discrete pockets of plastic strain in the layers of the softer material, as well as the wavelength of the wavy profile of the plastic strain in the harder material, are significantly smaller than the overall length of the layers. The plastic strain within all the discrete pockets in the layers of the softer material and along the entire waveform in the layers of the harder material initially continues to increase (see figures labeled 'ii' in Fig. 11) with increasing deformation. Next, with further increase in the imposed deformation (see figures labeled 'iii' in Fig. 11), the plastic strain increases more in a few select pockets in the layers of the softer material and at a few select locations along the waveform in the layers of the harder material resulting in localized plastic deformation at the specimen scale. Finally, the layers of both the materials within the localized plastic deformation band start to rotate

rapidly leading to the formation of a kink-band (see figures labeled 'iv' in Fig. 11). Note that as the kink-band forms, the layers of both the materials immediately outside the kink-band undergo unloading with the extent of unloading being greater in the layers of the softer material compared to that of the harder material, Figs. 10(B) and (b). Finally, once the kink-band is fully developed, continued deformation involves kink-band widening during which no further unloading is observed anywhere in the specimen and the deformation continues at roughly constant nominal stress (see Figs. 10C and c).

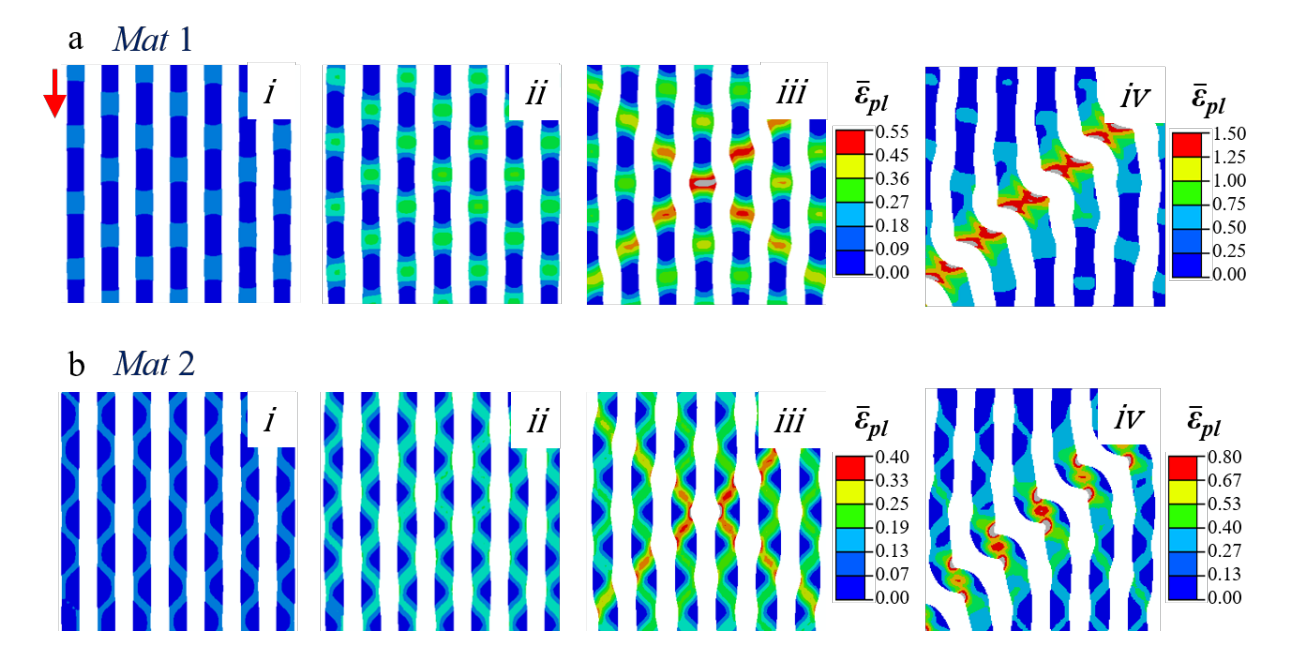


**Figure 11.** The distribution of effective plastic strain,  $\bar{\varepsilon}_{pl}$ , in the layers of (a) material 1 and that of (b) material 2 in the region marked with dashed boxes in Figs. 10A and a, respectively, at four imposed nominal compressive strain levels marked with dotted vertical lines (labeled *i-iv*) on the stress-strain curve shown in Fig. 10.

The full animation of the process of kink-band formation described with a few snapshots in Figs. 10 and 11 are provided in the Supplementary Movie S1. Furthermore, in the Supplementary Movie S2, a zoomed-in view of another region that did not eventually form kink-band is also shown. From the Supplementary Movie S2 it can be seen that in this region as well, the distribution of effective plastic strain and stress in the layers of the softer material is discrete while in the layers of the harder material is wavy before the onset of any macroscopic instability in the specimen. Also, the plastic strain and stress within all the discrete pockets in the layers of the softer material and along the entire wave-form in the layers of the harder material initially increase with increasing deformation. However, once a kink-band forms in the specimen, the layers of both the materials in the zoomed-in region shown in the Supplementary Movie S2 undergo unloading.

We also carried out parametric studies to understand the individual effects of layer thickness and the difference between the strength of the constituent materials on kink-band formation in the bimetallic layered composites. Our results demonstrate that there is a critical layer thickness below which, for a fixed value of strength differential between the layers of the constituent materials, the mode of deformation of the composite transitions from barreling to kink-band formation. Additionally, for a fixed layer thickness, there exists a critical value of the strength differential above which the same mode transition occurs. Our results also show that refining the layer thickness below the critical value as well as increasing the difference between the strength of the two materials above the critical value not only promotes early kink-band formation but also results in finer kink-bands. These effects result from both layer refinement and an increase in the strength differential, which contribute to enhanced local deformation heterogeneity and subsequently increase the propensity for instability. Furthermore, the results of our parametric studies

demonstrate that the extent of decrease in the nominal stress carrying capacity of the material after the initiation of kink-band formation primarily depends on the extent of strength differential between the strengths of the two materials in the composite specimens, rather than on the thickness of the layers.

Our parametric studies aimed at understanding the effects of materials' strain-hardenability on the kink-band formation in bimetallic layered composites show that increasing the strain-hardenability of the materials results in rather stable kink-band formation; and a simultaneous increase in both stress and strain levels at the onset of kink-band formation. More importantly, our results show that increasing the strain-hardenability of the materials in the bimetallic layered composites leads to a transition from the abrupt formation of through-width kink-band to onset and propagation of inclined wedge-shaped kink-bands across the width of the specimen (see Supplementary Movie S3). Similar kink-band onset and propagation sequence was observed in the experiments on Cu-Nb nanolayered composites (Nizolek et al., 2015). The inclined wedge-shaped kink-bands in the specimens are analogous to inclined-cracks with mixed Mode-I and Mode-II components as observed in the experiments (Nizolek et al., 2017).

The effects of materials' strain-hardenability on kink-band formation in bimetallic layered composites, as demonstrated here, differ somewhat from the observations made in fiber-reinforced polymeric composites (such as carbon fiber in an epoxy matrix or glass fiber in a polyester matrix). In the latter case, where the fiber-matrix elastic stiffness ratios are considerably higher, the strain-hardenability of the matrix material does not significantly impact the critical stress at the onset of kink-band formation (Budiansky and Fleck, 1993). Additionally, in fiber-reinforced polymeric

composites, the ultimate orientation and width of the kink-bands are primarily governed by the bending strength of the stiff fibers (Hsu et al., 1998).

We also carried out limited analyses of bimetallic layered composites subjected to layer normal compression. A representative result of these analyses is presented in Supplementary Figure S2. In this specific example, the composite had layer thicknesses of 30 nm for both materials. Material 1 had a yield strength of 700 MPa, while material 2 had a yield strength of 2000 MPa, in accordance with the Hall-Petch effect described in Section 3.1. The strain-hardening coefficient and exponent were set to 0.1 and 0.3, respectively, for both materials. As observed in the figure, during the initial stages of deformation, the specimen exhibits a linear stress-strain response, which is subsequently followed by a slight change in the slope of the curve. This transition is succeeded by macroscopic yielding. Post macroscopic yielding, the nominal stress-strain response of the material exhibits slight strain-hardening followed by eventual softening. Notably, despite the significant difference in strength between the two materials, co-deformation is observed locally in the layers of both materials, while macroscopically, the specimen initially deforms in a barrel-like fashion. As deformation continues, localization occurs in two intersecting shear-bands roughly inclined at ±45° with respect to the compression axis. These findings in Supplementary Figure S2 closely resemble experimental results by Snel et al. (2017) on Cu-Nb bimetallic layer composites with a layer thickness of 34 nm.

In our calculations, we assume that the layer thickness-dependent strength of the two constituent materials (Cu and Nb) in the bimetallic layered composites follows Hall-Petch relations, based on characterization performed using results obtained from bulk materials. This is because a separate

characterization of the effect of layer thickness on the yield strength of the constituent materials in the composite is currently unavailable. Although the grain morphology within the composite layers differs significantly from that of the bulk materials, the size-dependent macroscopic yield strength results obtained for the Cu-Nb layered composites in this work align with those observed experimentally in Nizolek et al. (2015) and Snel et al. (2017). This may be because both layer parallel and layer inclined slip in these composite materials contribute to their deformation (Zhang et al., 2022), and thus, assuming layer thickness as the critical size for Hall-Petch strengthening is seemingly sufficient to capture their size-dependent stress-strain response. Furthermore, in our calculations, the isotropic strain-hardenability of the constituent materials leads to the transition from the abrupt formation of through-width kink-bands to the onset and propagation of wedgeshaped kink-bands. However, it can be hypothesized that confined layer slip in the composite layers strongly depends on the orientation of the layers with respect to the compression axis. As the layers rotate (within the kink-band), the slip resistance within the layers evolves, resulting in anisotropic strain-hardening. This anisotropy can stabilize the kink-banding process and lead to the onset and propagation of stable kink-bands, as observed in experiments. To better capture the size and orientation-dependent strength and strain-hardenability of the constituent materials, a comprehensive non-local material model similar to that presented in Zecevic et al. (2023) can be utilized within the boundary value problem solved here. Such an analysis will also provide a deeper understanding of the microstructural evolution within the kink-bands, such as the accumulation of geometrically necessary dislocations and the formation of tilt geometrically necessary boundaries.

## 5. Concluding remarks

We carried out extensive plane strain finite element finite deformation calculations to understand and rationalize the experimentally observed kink-band formation in bimetallic layered composites when subjected to layer parallel compression. While we made assumptions to simplify the problem, several features of kink-band formation observed in the experiments such as the transition in the mode of deformation from barreling to kink-band formation with increasing layer refinement (i.e., decreasing layer thickness) naturally emerged in our calculations. These factors also naturally captured the formation of shear-bands in these composite materials when subjected to layer normal compression, as observed in the experiments. Additionally, we carried out parametric studies to understand the individual effects of layer thickness, strength differential between the two constituent materials and strain-hardenability of the materials on kink-band formation. The key conclusions of our work are as follows:

- Layer refinement, together with the strength differential between the layers of the constituent materials, alone constitutes 'sufficient conditions' to trigger kink-banding in bimetallic layered composites.
- The distribution of effective plastic strain in the individual layers of the constituent materials is remarkably distinct even before the onset of any instability. Specifically, the layers of the softer material exhibit a discrete distribution of plastic strain, while the layers of the harder material exhibit a wavy pattern. The interaction between these distinct local deformation patterns in the layers of the two materials eventually triggers the formation of kink-bands.

- For a fixed strength differential between the constituent materials, refining the layer thickness below a critical value, as well as increasing the strength differential above a critical value for a fixed layer thickness, not only promotes early kink-band formation but also results in the formation of finer kink-bands.
- The extent of decrease in the stress carrying capacity of the material after the onset of kinkband formation in bimetallic layered composites is found to depend significantly on the strength difference between the two materials rather than on the thickness of the layers.
- An increase in the strain-hardenability of the materials in bimetallic layered composites leads to a simultaneous increase in both stress and strain levels at the onset of kink-band formation. Moreover, increasing the strain-hardenability of the constituent materials induces a transition from the abrupt formation of through-width kink-bands to the onset and propagation of stable inclined wedge-shaped kink-bands.

We would like to note that, during the review process, an anonymous reviewer pointed out that the banding produced by the present analysis does not have the same characteristics as those of kinkbands in layered materials such as epoxy/fiber composites. According to the reviewer, the localization reported in the bimetallic composite specimens subjected to layer parallel compression in the present work appears to be closer to shear-bands.

#### **Declaration of competing interest**

The authors declare that they have no known competing financial interests or personal relationships that could have appeared to influence the work reported in this paper.

## Data availability

Data will be made available on request.

#### Acknowledgement

The financial support provided by the U.S. National Science Foundation grant CMMI-1944496 is gratefully acknowledged. The finite element calculations reported on were carried out using the high-performance research computing resources provided by the Texas A&M University.

#### References

Anderson, P., Foecke, T., Hazzledine, P., 1999. Dislocation-based deformation mechanisms in metallic nanolaminates. Mrs Bulletin 24, 27-33.

Anderson, T., 1968. The geometry of natural ortho-rhombic systems of kink bands. Geol. Surv. Canada Paper 68, 200-225.

Ardeljan, M., Knezevic, M., Jain, M., Pathak, S., Kumar, A., Li, N., Mara, N.A., Baldwin, J.K., Beyerlein, I.J., 2018. Room temperature deformation mechanisms of Mg/Nb nanolayered composites. Journal of Materials Research 33, 1311-1332.

Ardeljan, M., Knezevic, M., Nizolek, T., Beyerlein, I., Zheng, S., Carpenter, J., McCabe, R., Mara, N., Pollock, T., 2014. A multi-scale model for texture development in Zr/Nb nanolayered composites processed by accumulative roll bonding, IOP Conference Series: Materials Science and Engineering. IOP Publishing, p. 012170.

Argon, A., 2013. Fracture of composites. Treatise on materials science and technology 1, 79-114.

Arora, A., Arora, R., Acharya, A., 2023. Interface-dominated plasticity and kink bands in metallic nanolaminates. Crystals 13, 828.

Attenburrow, G., Bassett, D., 1979. Compliances and failure modes of oriented chain-extended polyethylene. Journal of Materials Science 14, 2679-2687.

Barsoum, M., Zhen, T., Kalidindi, S., Radovic, M., Murugaiah, A., 2003. Fully reversible, dislocation-based compressive deformation of Ti 3 SiC 2 to 1 GPa. Nature Materials 2, 107-111.

Barsoum, M.W., Radovic, M., 2011. Elastic and mechanical properties of the MAX phases. Annual review of materials research 41, 195-227.

Berg, C., Salama, M., 1973. Fatigue of graphite fibre-reinforced epoxy in compression. Fibre Science and Technology 6, 79-118.

Beyerlein, I., Caro, A., Demkowicz, M., Mara, N., Misra, A., Uberuaga, B., 2013a. Radiation damage tolerant nanomaterials. Materials today 16, 443-449.

Beyerlein, I.J., Mara, N.A., Carpenter, J.S., Nizolek, T., Mook, W.M., Wynn, T.A., McCabe, R.J., Mayeur, J.R., Kang, K., Zheng, S., 2013b. Interface-driven microstructure development and ultra high strength of bulk nanostructured Cu-Nb multilayers fabricated by severe plastic deformation. Journal of materials research 28, 1799.

Budiansky, B., 1983. Micromechanics. Computers & Structures 16, 3-12.

Budiansky, B., Fleck, N.A., 1993. Compressive failure of fibre composites. Journal of the Mechanics and Physics of Solids 41, 183-211.

Carpenter, J., Liu, X., Darbal, A., Nuhfer, N., McCabe, R., Vogel, S., LeDonne, J., Rollett, A., Barmak, K., Beyerlein, I., 2012. A comparison of texture results obtained using precession electron diffraction and neutron diffraction methods at diminishing length scales in ordered bimetallic nanolamellar composites. Scripta Materialia 67, 336-339.

Carpenter, J., Nizolek, T., McCabe, R., Zheng, S., Scott, J., Vogel, S., Mara, N., Pollock, T., Beyerlein, I., 2015. The suppression of instabilities via biphase interfaces during bulk fabrication of nanograined Zr. Materials Research Letters 3, 50-57.

Carpenter, J., Zheng, S., Zhang, R., Vogel, S., Beyerlein, I., Mara, N., 2013. Thermal stability of Cu–Nb nanolamellar composites fabricated via accumulative roll bonding. Philosophical Magazine 93, 718-735.

Carpenter, J.S., McCabe, R.J., Zheng, S.J., Wynn, T.A., Mara, N.A., Beyerlein, I.J., 2014. Processing parameter influence on texture and microstructural evolution in Cu-Nb multilayer composites fabricated via accumulative roll bonding. Metallurgical and Materials Transactions A 45, 2192-2208.

Chen, T., Yuan, R., Beyerlein, I.J., Zhou, C., 2020. Predicting the size scaling in strength of nanolayered materials by a discrete slip crystal plasticity model. International Journal of Plasticity 124, 247-260.

Cordero, Z.C., Knight, B.E., Schuh, C.A., 2016. Six decades of the Hall–Petch effect–a survey of grain-size strengthening studies on pure metals. International Materials Reviews 61, 495-512.

Cornwell, L., Embury, J., Purdy, G., 1970. The deformation of single crystals of the Ni□ Ni3Al system. Acta Metallurgica 18, 1217-1223.

Crocker, A., Abell, J., 1976. The crystallography of deformation kinking. Philosophical Magazine 33, 305-310.

Del Valle, J., Pérez-Prado, M.T., Ruano, O.A., 2005. Accumulative roll bonding of a Mg-based AZ61 alloy. Materials Science and Engineering: A 410, 353-357.

Dewey, J., 1965. Nature and origin of kink-bands. Tectonophysics 1, 459-494.

Evans, A., Adler, W., 1978. Kinking as a mode of structural degradation in carbon fiber composites. Acta Metallurgica 26, 725-738.

Fleck, N., Budiansky, B., 1991. Compressive failure of fibre composites due to microbuckling, Inelastic deformation of composite materials. Springer, pp. 235-273.

Frank, F., Stroh, A., 1952. On the theory of kinking. Proceedings of the Physical Society. Section B 65, 811.

Hagihara, K., Mayama, T., Honnami, M., Yamasaki, M., Izuno, H., Okamoto, T., Ohashi, T., Nakano, T., Kawamura, Y., 2016. Orientation dependence of the deformation kink band formation behavior in Zn single crystal. International Journal of Plasticity 77, 174-191.

Hall, E., 1951. The deformation and ageing of mild steel: III discussion of results. Proceedings of the Physical Society. Section B 64, 747.

Han, W., Cerreta, E., Mara, N., Beyerlein, I., Carpenter, J., Zheng, S., Trujillo, C., Dickerson, P., Misra, A., 2014. Deformation and failure of shocked bulk Cu–Nb nanolaminates. Acta Materialia 63, 150-161.

Han, W., Demkowicz, M.J., Mara, N.A., Fu, E., Sinha, S., Rollett, A.D., Wang, Y., Carpenter, J.S., Beyerlein, I.J., Misra, A., 2013. Design of radiation tolerant materials via interface engineering. Advanced materials 25, 6975-6979.

Hess, J., Barrett, C., 1949. Structure and nature of kink bands in zinc. Jom 1, 599-606.

Hong, C., Tao, N., Huang, X., Lu, K., 2010. Nucleation and thickening of shear bands in nanoscale twin/matrix lamellae of a Cu–Al alloy processed by dynamic plastic deformation. Acta Materialia 58, 3103-3116.

Hsu, S.-Y., Vogler, T., Kyriakides, S., 1998. Compressive strength predictions for fiber composites.

Jensen, H.M., Christoffersen, J., 1997. Kink band formation in fiber reinforced materials. Journal of the Mechanics and Physics of Solids 45, 1121-1136.

Jian, W.-R., Xu, S., Su, Y., Beyerlein, I.J., 2022. Role of layer thickness and dislocation distribution in confined layer slip in nanolaminated Nb. International Journal of Plasticity 152, 103239.

Kronenberg, A.K., Kirby, S.H., Pinkston, J., 1990. Basal slip and mechanical anisotropy of biotite. Journal of Geophysical Research: Solid Earth 95, 19257-19278.

Kyriakides, S., Arseculeratne, R., Perry, E., Liechti, K., 1995. On the compressive failure of fiber reinforced composites. International journal of solids and structures 32, 689-738.

Manley, M., Schulson, E., 1997. Kinks and cracks in S1 ice under across-column compression. Philosophical magazine letters 75, 83-90.

Mara, N., Bhattacharyya, D., Dickerson, P., Hoagland, R., Misra, A., 2008. Deformability of ultrahigh strength 5 nm Cu/Nb nanolayered composites. Applied Physics Letters 92, 231901.

Mara, N., Bhattacharyya, D., Hirth, J., Dickerson, P., Misra, A., 2010a. Mechanism for shear banding in nanolayered composites. Applied Physics Letters 97, 021909.

Mara, N.A., Beyerlein, I.J., 2014. effect of bimetal interface structure on the mechanical behavior of Cu–Nb fcc–bcc nanolayered composites. Journal of materials science 49, 6497-6516.

Mara, N.A., Bhattacharyya, D., Dickerson, P.O., Hoagland, R., Misra, A., 2010b. Ultrahigh strength and ductility of Cu-Nb nanolayered composites, Materials Science Forum. Trans Tech Publ, pp. 647-653.

Misra, A., Demkowicz, M., Zhang, X., Hoagland, R., 2007. The radiation damage tolerance of ultra-high strength nanolayered composites. Jom 59, 62-65.

Misra, A., Hirth, J., Hoagland, R., 2005. Length-scale-dependent deformation mechanisms in incoherent metallic multilayered composites. Acta materialia 53, 4817-4824.

Misra, A., Hoagland, R., Kung, H., 2004. Thermal stability of self-supported nanolayered Cu/Nb films. Philosophical Magazine 84, 1021-1028.

Misra, A., Verdier, M., Lu, Y., Kung, H., Mitchell, T., Nastasi, M., Embury, J., 1998. Structure and mechanical properties of Cu-X (X= Nb, Cr, Ni) nanolayered composites. Scripta Materialia 39, 555-560.

Moran, P., Liu, X., Shih, C., 1995. Kink band formation and band broadening in fiber composites under compressive loading. Acta metallurgica et Materialia 43, 2943-2958.

Nestorović, M., Triantafyllidis, N., 2004. Onset of failure in finitely strained layered composites subjected to combined normal and shear loading. Journal of the Mechanics and Physics of Solids 52, 941-974.

Nizolek, T., Begley, M., McCabe, R., Avallone, J., Mara, N., Beyerlein, I., Pollock, T., 2017. Strain fields induced by kink band propagation in Cu-Nb nanolaminate composites. Acta Materialia 133, 303-315.

Nizolek, T., Mara, N.A., Beyerlein, I.J., Avallone, J.T., Pollock, T.M., 2015. Enhanced plasticity via kinking in cubic metallic nanolaminates. Advanced Engineering Materials 17, 781-785.

Nizolek, T.J., 2016. Plastic Anisotropy and Kink Band Formation in Fine Grained Copper-Niobium Multilayers Produced by Accumulative Roll Bonding. University of California, Santa Barbara, United States -- California, p. 332.

Nizolek, T.J., Pollock, T.M., McMeeking, R.M., 2021. Kink band and shear band localization in anisotropic perfectly plastic solids. Journal of the Mechanics and Physics of Solids 146, 104183.

Orowan, E., 1942. A TYPE OF PLASTIC DEFORMATION NEW IN METALS. Nature 149, 643-644.

Paterson, M., Weiss, L., 1966. Experimental deformation and folding in phyllite. Geological Society of America Bulletin 77, 343-374.

Petch, N.J., 1953. The Cleavage Strength of Polycrystals. J Iron Steel I 174, 25-28.

Plummer, G., Rathod, H., Srivastava, A., Radovic, M., Ouisse, T., Yildizhan, M., Persson, P.Å., Lambrinou, K., Barsoum, M., Tucker, G., 2021. On the origin of kinking in layered crystalline solids. Materials Today.

Poulsen, J.S., Moran, P., Shih, C., Byskov, E., 1997. Kink band initiation and band broadening in clear wood under compressive loading. Mechanics of materials 25, 67-77.

Rathod, H.J., Ouisse, T., Radovic, M., Srivastava, A., 2021. Room temperature crack-healing in an atomically layered ternary carbide. Science Advances 7, eabg2549.

Robertson, R.E., 1969. Formation of kink bands in oriented polymers. Journal of Polymer Science Part A-2: Polymer Physics 7, 1315-1328.

Rosen, B.W., 1970. Strength of uniaxial fibrous composites, Mechanics of composite materials. Elsevier, pp. 621-651.

Saito, Y., Utsunomiya, H., Tsuji, N., Sakai, T., 1999. Novel ultra-high straining process for bulk materials—development of the accumulative roll-bonding (ARB) process. Acta materialia 47, 579-583.

Snel, J., Monclús, M., Castillo-Rodriguez, M., Mara, N., Beyerlein, I., Llorca, J., Molina-Aldareguia, J.M., 2017. Deformation mechanism map of Cu/Nb nanoscale metallic multilayers as a function of temperature and layer thickness. Jom 69, 2214-2226.

Subedi, S., Beyerlein, I.J., LeSar, R., Rollett, A.D., 2018. Strength of nanoscale metallic multilayers. Scripta Materialia 145, 132-136.

Tian, Y., Zhang, Z., 2013. Stability of interfaces in a multilayered Ag–Cu composite during cold rolling. Scripta Materialia 68, 542-545.

Triantafyllidis, N., Maker, B., 1985. On the comparison between microscopic and macroscopic instability mechanisms in a class of fiber-reinforced composites.

Valiev, R.Z., Langdon, T.G., 2006. Principles of equal-channel angular pressing as a processing tool for grain refinement. Progress in materials science 51, 881-981.

Vogler, T., Hsu, S.-Y., Kyriakides, S., 2001. On the initiation and growth of kink bands in fiber composites. Part II: analysis. International Journal of Solids and Structures 38, 2653-2682.

Vogler, T., Kyriakides, S., 2001. On the initiation and growth of kink bands in fiber composites: Part I. experiments. International journal of solids and structures 38, 2639-2651.

Wang, J., Misra, A., 2014. Strain hardening in nanolayered thin films. Current Opinion in Solid State and Materials Science 18, 19-28.

Xue, Q., Beyerlein, I., Alexander, D., Gray Iii, G., 2007. Mechanisms for initial grain refinement in OFHC copper during equal channel angular pressing. Acta Materialia 55, 655-668.

Yan, J., Zhu, X., Yang, B., Zhang, G., 2013. Shear stress-driven refreshing capability of plastic deformation in nanolayered metals. Physical review letters 110, 155502.

Zecevic, M., Lebensohn, R.A., Capolungo, L., 2022. New large-strain FFT-based formulation and its application to model strain localization in nano-metallic laminates and other strongly anisotropic crystalline materials. Mechanics of Materials, 104208.

Zecevic, M., Lebensohn, R.A., Capolungo, L., 2023. Non-local large-strain FFT-based formulation and its application to interface-dominated plasticity of nano-metallic laminates. Journal of the Mechanics and Physics of Solids 173, 105187.

Zhang, Y., Li, N., Schneider, M.M., Nizolek, T.J., Capolungo, L., McCabe, R.J., 2022. Kink mechanism in Cu/Nb nanolaminates explored by in situ pillar compression. Acta Materialia 237, 118150.

Zheng, S., Wang, J., Carpenter, J., Mook, W., Dickerson, P., Mara, N., Beyerlein, I., 2014. Plastic instability mechanisms in bimetallic nanolayered composites. Acta materialia 79, 282-291.

## Supplementary Materials for:

# Micromechanics of kink-band formation in bimetallic layered composites

Hemant J. Rathod, Umair Bin Asim, Miladin Radovic, Ankit Srivastava\* Department of Materials Science and Engineering, Texas A&M University, College Station, TX 77845, USA

## \*Corresponding author.

Email address: ankit.sri@tamu.edu (A. Srivastava)

## This file includes:

Supplementary Figures S1 and S2 Captions for Supplementary Movies S1 to S3

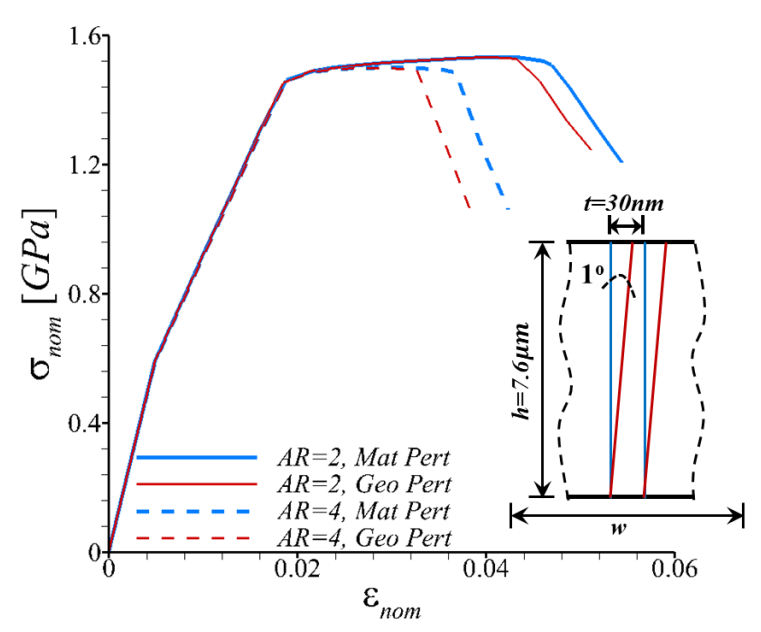


**Figure S1.** A comparison of the effects of material (Mat) and geometric (Geo) perturbations (Pert) on the nominal compressive stress-strain response is presented for two bimetallic layered composite specimens with aspect ratios AR (h/w) of 2 and 4. These specimens were subjected to layer-parallel compression under identical boundary and loading conditions, as described in Section 2 of the manuscript. For both specimens, the layer thicknesses of both materials are 30 nm. The yield strength of material 1 is 500 MPa, while that of material 2 is 2000 MPa. Both materials have a strain-hardening coefficient, K = 0.1, and an exponent, n = 0.3.

The material perturbation implies a random  $\pm 1\%$  perturbation in the values of  $\sigma_y$  of the individual layers, while the geometrical perturbation implies a one-degree tilt in the interfaces between the layers of materials 1 and 2, as shown schematically in the figure insert.

The nominal strain ( $\varepsilon_{nom}$ ) at the drop in the load-carrying capacity for the specimen with AR=2 subjected to geometrical perturbation is 7% less than that with material perturbation, while for the specimen with AR=4, it is 12% less.

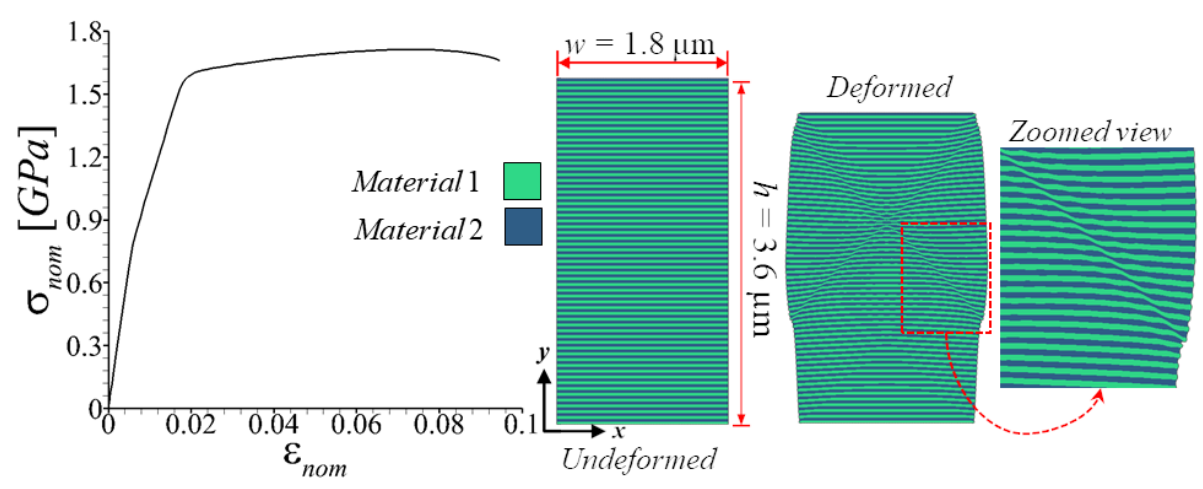


**Figure S2.** From left to right: Nominal compressive stress-strain response of a bimetallic layered composite specimen subjected to layer normal compression. Schematic representation of a plane strain finite element model of a bimetallic layered composite subjected to layer normal compression. Deformed shape of the specimen at an imposed nominal strain of 0.1. Zoomed view of the deformed shape revealing the formation of a shear band. The layer thicknesses of both materials are 30 nm, and their material properties are the same as described in Section 3.1 of the manuscript.

The overall in-plane dimensions, height (h) and width (w), of the specimen modeled are 3.6  $\mu$ m and 1.8  $\mu$ m, respectively, giving an aspect ratio (h/w) of 2. The deformation of the specimen is constrained in both the x and y directions on the bottom surface (y=0 surface), and only in the x direction on the top surface  $(y=3.6 \mu\text{m})$  in the reference configuration). The top surface is subjected to deformation along the y-axis. All other aspects of the numerical method are the same as described in Section 2 of the manuscript.

**Movie S1 (Supplementary video 2).** Full animation of kink-band formation in a specimen of a bimetallic layered composite together with the zoomed-in views of a small region that is eventually engulfed by the kink-band. In the bimetallic layered composite specimen shown here, the thickness of all layers is 30 nm, the yield strength of materials 1 and 2 is 500 MPa and 2000 MPa, respectively, and the strain-hardening coefficient and exponent for both the materials are 0.1 and 0.3, respectively. (a) The evolution of effective plastic strain. (b) The evolution of effective stress. (c) Nominal compressive stress-strain response of the specimen. (d)-(e) The evolution of effective plastic strain and effective stress in the layers of material 1 and (f)-(g) that of material 2 in the region marked with a dashed box in Figs. (a) and (b).

Movie S2 (Supplementary video 3). Full animation of kink-band formation in a specimen of a bimetallic layered composite together with the zoomed-in views of a small region away from the kink-band. In the bimetallic layered composite specimen shown here, the thickness of all layers is 30 nm, the yield strength of materials 1 and 2 is 500 MPa and 2000 MPa, respectively, and the strain-hardening coefficient and exponent for both the materials are 0.1 and 0.3, respectively. (a) The evolution of effective plastic strain. (b) The evolution of effective stress. (c) Nominal compressive stress-strain response of the specimen. (d)-(e) The evolution of effective plastic strain and effective stress in the layers of material 1 and (f)-(g) that of material 2 in the region marked with a dashed box in Figs. (a) and (b).

Movie S3 (Supplementary video 4). Full animation of kink-band nucleation and growth in a specimen of a bimetallic layered composite together with the zoomed-in views of two small regions further showing nucleation and growth of the kink-band. In the bimetallic layered composite specimen shown here, the thickness of all layers is 30 nm, the yield strength of materials 1 and 2 is 500 MPa and 2000 MPa, respectively, and the strain-hardening coefficient and exponent for both the materials are 1.0 and 0.3, respectively. (a) The evolution of effective stress. (b) The evolution of effective plastic strain. (c) Nominal compressive stress-strain response of the specimen. (d)-(e) The zoomed-in views of the progressive deformation and evolution of effective plastic strain in the regions marked with dashed boxes in Fig. (b).